Broadening and line mixing in the 20 0 0←01 1 0, 11 1 0←00 0 0 and 12 2 0←01 1 0 Q branches of carbon dioxide: Experimental results and energy-corrected sudden modeling

A. Predoi-Cross, A. D. May, A. Vitcu, J. R. Drummond, J.-M. Hartmann, and C. Boulet

Citation: The Journal of Chemical Physics **120**, 10520 (2004); doi: 10.1063/1.1738101
View online: http://dx.doi.org/10.1063/1.1738101
View Table of Contents: http://scitation.aip.org/content/aip/journal/jcp/120/22?ver=pdfcov
Published by the AIP Publishing

Broadening and line mixing in the $20^00 \leftarrow 01^10$, $11^10 \leftarrow 00^00$ and $12^20 \leftarrow 01^10$ Q branches of carbon dioxide: Experimental results and energy-corrected sudden modeling

A. Predoi-Cross[a)]
Physics Department, The University of Lethbridge, 4401 University Drive, Lethbridge, AB, T1K 3M4 Canada

A. D. May, A. Vitcu, and J. R. Drummond
Department of Physics, University of Toronto, Toronto, ON, M5S 1A7 Canada

J.-M. Hartmann and C. Boulet
Laboratoire de Photophysique Moleculaire, Bâtiment 210, Université Paris-Sud, F-91405, Orsay Cedex, France

(Received 9 February 2004; accepted 16 March 2004)

Using both a difference frequency spectrometer and a Fourier transform spectrometer, we have measured transitions in the $12^20 \leftarrow 01^10$ band of carbon dioxide at room temperature and pressures up to 19 atm. The low-pressure spectra were analyzed using a variety of standard spectral profiles, all with an asymmetric component to account for weak line mixing. For this band, we have been able to retrieve experimental line strengths and the broadening and weak mixing parameters. In this paper we also compare the suitability of the energy-corrected sudden model to predict mixing in the two previously measured Q branches $20^00 \leftarrow 01^10$, the $11^10 \leftarrow 00^00$, and the present Q branch of pure CO_2, all at room temperature. © *2004 American Institute of Physics.*
[DOI: 10.1063/1.1738101]

I. INTRODUCTION

Carbon dioxide is present in the atmospheres of all three ''Earth-like'' planets in our solar system. While on Earth the gas is diluted to 0.04% with N_2 or O_2, on Mars and Venus it is the dominant component at about the 95% level for both planets. CO_2 (partial) pressures vary from extremely low values in the upper atmospheres of the planets, to 5 torr at the surface of Mars, 760 torr at the surface of Earth, and 70 000 torr (90 atm) at the surface of Venus. In order to understand the radiative properties of these atmospheres, the spectral characteristics of CO_2 must be known over a similarly large range of pressures and the ultimate goal is to have a single theory or model that can predict the emission/absorption features over this entire range of pressures.

It is well known that modeling of the shape of absorption due to clusters of lines, such as Q branches or manifolds, often requires accounting for the influence of line mixing[1] when the pressure is such that the spectral contributions of the various transitions overlap significantly. The need to account for line mixing in forward calculations of absorption/emission of CO_2 in the Earth's atmosphere has been demonstrated.[2–5] In the case of CO_2, Q branches line mixing has received considerable experimental and theoretical attention in the infrared. Many laboratory measurements have been made for mixtures with N_2 or other gases, whereas pure CO_2 has received less attention.[6–12] Here, we complete our series of measurements[6,7] of broadening and mixing by presenting, in Part I, results for the $12^20 \leftarrow 01^10$ band ($\Delta \leftarrow \Pi$ transition) at 2093 cm^{-1}. As distinct from the earlier papers, this $\Delta \leftarrow \Pi$ transition possesses vibrational angular momentum in both the lower ($l=1$) and the upper ($l=2$) state. In such a case both the structure of the band and mixing is more complex than is found for simple Q branches.

Various approaches have been proposed for the modeling of line mixing: they include simple empirical approaches,[13] semiclassical models,[14] the use of fitting[12,15] and scaling[11,16] laws, and first principle calculations starting from the intermolecular potential.[17] Among the models tractable for precise modeling the absorption shape of Q branches, the scaling approach based on the energy-corrected Sudden approximation (ECS) has been widely and successfully used for a number of molecular systems.[4,6,18–21] When compared with other fitting laws it has the advantage of including, explicitly and intrinsically, the influence of the vibrational symmetry (angular momentum) of the band and of the branches to which the lines belong, and of applying to all bands of a given molecular system simultaneously. Its performance has been widely demonstrated in Q branches or entire bands for CO_2–(N_2, O_2, air,...) mixtures, but few tests[11,22] have been made for pure CO_2. Here, in Part II, we test it for the three Q branches of pure CO_2, the $\Pi \leftarrow \Sigma$ transition ($11^10 \leftarrow 00^00$) at 2077 cm^{-1}, the $\Sigma \leftarrow \Pi$ transition ($20^00 \leftarrow 01^10$) at 2130 cm^{-1}, and the present $\Delta \leftarrow \Pi$ transition ($12^20 \leftarrow 01^10$) located at 2093 cm^{-1}. However, before proceeding to Parts I and II, it is worthwhile to give a brief outline of the theory of line mixing.

Disregarding Doppler and velocity effects,[23,24] the collisional absorption coefficient for pure CO_2 under total pressure P and temperature T is given, within the impact approximation, by[25]

[a)]Electronic mail: adriana.predoicross@uleth.ca

$$\alpha(\sigma,P,T)=\frac{8\pi^2}{3hc}\sigma\left[1-\exp\left(\frac{-hc\sigma}{k_BT}\right)\right]\frac{P}{k_BT}\times\sum_k\sum_{k'}\rho_k(T)\times d_k d_{k'}\{\langle k'|(\Sigma-L_o-iPw(T))^{-1}|k\rangle\}. \quad (1)$$

The sum extends over all CO_2 lines k and k', and Im{...} denotes the imaginary part, while ρ_k and d_k are the population of the initial level of line k and the dipole matrix element of the optical transition, respectively. Σ, L_0, and $W=Pw$ are operators in the Liouville (line) space. The first two are diagonal and associated with the wave number σ of the calculation and the positions σ_k of the unperturbed lines ($\langle\langle k'|\Sigma|k\rangle\rangle=\delta_{k,k'}\times\sigma$ and $\langle\langle k'|L_0|k\rangle\rangle=\delta_{k,k'}\times\sigma_k$). The relaxation operator w, per unit of pressure, accounts for the effects of CO_2-CO_2 collisions. The diagonal elements [which are the broadening, (γ_k), and shifting (δ_k), coefficients of individual lines] are related to the off-diagonal line-coupling terms by the sum rule

$$\gamma_k-i\,\delta_k=\langle\langle k|w|k\rangle\rangle=-\sum_{k'\neq k}\frac{d^o_{k'}}{d^o_k}\langle\langle k'|w|k\rangle\rangle, \quad (2)$$

where d^o_k and $d^o_{k'}$ are the unperturbed (rigid rotor) dipole reduced matrix elements.[26]

It is well known[27,28] that diagonalizing (L_0+iPw) allows one to write Eq. (1) as a single sum of asymmetric Lorentzian components, I_k

$$I_k(\sigma)=\frac{S_k}{\pi}\left[\frac{\Gamma_k}{(\sigma-\sigma_k-\Delta_k)^2+\Gamma_k^2}+Y_k\frac{(\sigma-\sigma_k-\Delta_k)}{(\sigma-\sigma_k-\Delta_k)^2+\Gamma_k^2}\right], \quad (3)$$

where S_k is the strength, σ_k is the center position, Γ_k is the Lorentz half-width at half-maximum (HWHM), Y_k is the line-mixing parameter, and Δ_k is the pressure shift of the kth component.

While the relaxation matrix, $W=Pw$, is linear in pressure, in Eq. (3) the strength, asymmetry, width, and shift are all complicated functions of the pressure. Furthermore, it is only at low densities that one can think of the spectral components, k, as being a physically meaningful line. For instance, as we shall see below, it is possible for the strength of a spectral component to be negative.

When line mixing is neglected, w is diagonal, and Eq. (1) reduces to a sum of symmetric Lorentzian profiles. The positions, widths, and intensities of the isolated lines vary with pressure. Furthermore, a low-pressure, first-order development of Eq. (1) or (3), valid in the case of weak overlapping ($|\sigma_k-\sigma_{k'}|\gg|P\langle\langle k|w|k\rangle\rangle|$), leads to[29]

$$\alpha(\sigma,P,T)=\frac{8\pi^2}{3hc}\sigma\left[1-\exp\left(\frac{-hc\sigma}{k_BT}\right)\right]\frac{P}{k_BT}\sum_k\rho_k(T)d_k^2\times\mathrm{Im}\left\{\frac{1+iPy_k(T)}{\sigma-\sigma_k-iP\langle\langle k|w(T)|k\rangle\rangle}\right\}, \quad (4)$$

with, y_k, the weak mixing coefficient, being given by

$$y_k(T)=2\sum_{k'\neq k}\frac{d_{k'}}{d_k}\frac{\langle\langle k'|w(T)|k\rangle\rangle}{\sigma_k-\sigma_{k'}}. \quad (5)$$

Here, in contrast to Eq. (3), each asymmetric *component* is a *line* and the mixing parameter Y_k is now proportional to pressure ($Y_k=P\ y_k$).

II. PART I

A. Experimental details

All of the experiments presented here were carried out at the University of Toronto. We have used a difference frequency laser spectrometer to record CO_2 spectra below 1 atmosphere. We give only a brief outline of the system as it has been described elsewhere.[30] The infrared radiation tunable from 2.5 to 5.5 μm is obtained by overlapping and mixing the light from two single-frequency lasers in a $LiIO_3$ crystal. The infrared power is normalized by splitting the infrared beam and monitoring the input and output signals from the following absorption cell with two identical LN_2-cooled, InSb detectors. The frequency measurement subsystem has as its principal component a temperature-stabilized, scanning Fabry–Perot interferometer used to determine the frequencies of both the dye and the argon ion laser relative to the frequency of a stabilized HeNe laser. Using phase sensitive detection we can achieve a resolution of about 2 MHz (6×10^{-5} cm^{-1}) and a signal-to-noise ratio close to 1500:1 for a 1 s integration time.

We have used temperature-controlled gas cells of 1 and 4 m length. The temperature was monitored and stabilized at 296.2 K with a precision of ±0.4 K using an Omega temperature controller. We have tried to minimize the temperature gradients along the cell by attaching additional heating coils to the end flanges. To avoid etaloning effects in the optics, the cell and detectors had Brewster CaF_2 windows and the $LiIO_3$ crystal was antireflection coated. For both cells the maximum variation of the empty cell transmission (baseline signal) was 1 part in 500 for a 1 cm^{-1} scan. The gas pressure was monitored using an MKS 120 AA capacitance manometer, calibrated by the manufacturer to an absolute accuracy of 0.05% of the full scale reading.

The high-pressure spectra presented in this work were recorded using a Bomem DA8.003 Fourier transform spectrometer and a 25 cm long temperature-controlled cell able to stand gas pressures up to 30 atm. The short cell had CaF_2 windows. The detector used was an InSb detector with a cold filter. The CO_2 spectra were recorded at 0.004 cm^{-1} resolution and the signal-to-noise ratio was in excess of 1000:1. We have used an iris aperture of 0.5 mm. The instrumental line shape was much smaller than the width of the collapsed Q branches and has been ignored in our high-pressure FTIR spectra. The FTIR measurements were made at 303.2 K. As above, the temperature was monitored and stabilized using an Omega temperature controller. The gas sample used in all experiments was supplied by Matheson and had a purity of 99.99%.

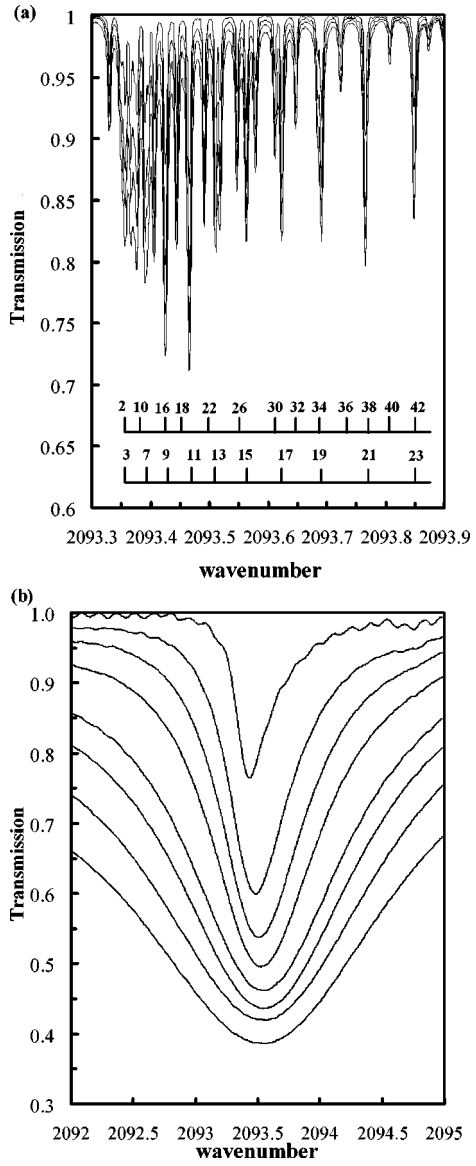

FIG. 1. (a) Several transmittance spectra of pure CO_2 at low pressure; (b) overlaid high-pressure FTIR spectra at pressures from 1 to 19 atm.

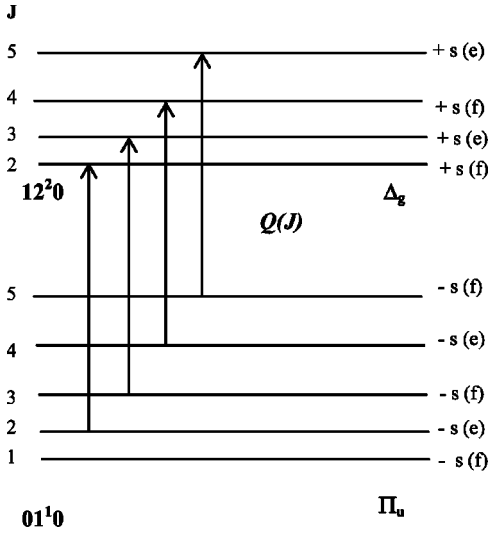

FIG. 2. Total parity ($\pm$) and rotationless parity (e/f) of the $12\,^20 \leftarrow 01\,^10$ Q branch.

B. Results and discussion

Figure 1(a) shows sample transmission spectra of the $12\,^20 \leftarrow 01\,^10$ band of carbon dioxide at low pressure. In the figure, the experimental points have been joined by straight line sections. As explained below, the 1-type doubling leads to a doubling of the band, the even J lines being clustered near 2093.4 cm^{-1} while the odd J lines are spread out towards higher frequency. As illustrated in Fig. 1(b), the entire band collapses to a single profile at high pressure. It is only at low pressures that one can extract values of pressure broadening and line-mixing coefficients. We analyze the low-pressure data (5–20 torr) in an iterative manner, exactly as in the earlier publication.[7] In the fitting routine we have used several well-known line shapes, all with an asymmetric component to allow for weak line mixing. In the first step we extract line strengths and approximate linewidths from the data. In the second step we extract accurate widths and approximate mixing coefficients. In the final step, accurate line-mixing parameters are determined. At each step we correct the data using calculated values of the next higher term arising from line mixing. In order to calculate the mixing terms, we need a relaxation matrix, w. As in Ref. 7, we use the EPG law proposed by Strow.[3] A fundamental assumption made in the model is that all of the broadening and mixing arises from rotationally inelastic collisions within a given vibrational manifold.

Knowledge of the level structure is necessary for understanding the effect of rotationally inelastic collisions on the line mixing. $^{12}C^{16}O_2$ belongs to the point group D_∞. Herzberg (Ref. 31, p. 373) has given a generic energy level diagram for such molecules. However, ^{16}O is a boson with zero nuclear spin and thus only the symmetric (s) states exist for our case. Consequently, as illustrated in Fig. 2, the rotational levels in the Π_u vibrational state all have the same negative ($-$) total parity, while in the Δ_g vibrational state all have positive ($+$) total parity. What is important for this paper is the fact that in each state the even J levels all belong to either the upper or the lower of the two 1-type doublets, while the reverse is true for the odd J levels. Thus, the even J levels have one effective rotational constant (B) while the odd J levels have a different value for the effective B. Hence, the ΔB, describing the spreading of the Q branch, has two values, one for J even and another for J odd, exactly as illustrated in Fig. 1(a). Our earlier publications[6,7] involved Σ states for which only J even levels exist. It is convenient to introduce a ''rotationless'' parity (to distinguish the two possible 1-type doublets) by removing from the total parity, the usual rotational factor $(-1)^J$. The even/odd rotationless parity states are conventionally designated by e/f.[32] We have added these labels to the states in Fig. 2. We see in both vibrational states that the even J levels have one rotationless parity while the odd J levels have the other rotationless parity. If only the J even and only the J odd levels were coupled by collisions (ΔJ even), line mixing would occur only within each sub-Q branch. As we shall see, there exists strong experimental evidence that both ΔJ even and ΔJ odd

collisional transfer exist, and thus we consider a form of the EPG law that allows for this possibility. In the rest of this paper we will refer to rotationless parity simply as parity.

The EPG law gives the collisional transfer rate, k_{jk}, from a rotational state k to a higher rotational state j as

$$k_{jk}=a\left[\frac{|\Delta E_{jk}|}{B_o}\right]^{-b}\exp\left[-c\,\frac{|\Delta E_{jk}|}{k_BT}\right], \tag{6}$$

where ΔE_{jk} is the rotational energy difference between the two states and B_o is the rotational constant, all within a given vibrational level. The adjustable parameters of the model are a, b, and c. The rates of population transfer must satisfy the detailed balance condition

$$\rho_k k_{jk}=\rho_j k_{kj}, \tag{7}$$

where ρ_k is the population of the rotational state, k.

In our version of the EPG model, we allow for collisions with ΔJ both odd and even, i.e., with and without parity changes (Ref. 33 and references therein), by writing the diagonal elements of the relaxation matrix for transitions in the $12\,^20\leftarrow01\,^10$ Q branch of $^{12}C^{16}O_2$ as

$$w_{kk}=\frac{1}{2}\left\{\sum_{\substack{j\neq k\\ \text{same parity}}}\beta_\Pi k_{jk}+\sum_{\substack{j\neq k\\ \text{different parity}}}(1-\beta_\Pi)k_{jk}\right\}+\frac{1}{2}\left\{\sum_{\substack{j\neq k\\ \text{same parity}}}\beta_\Delta k_{jk}+\sum_{\substack{j\neq k\\ \text{different parity}}}(1-\beta_\Delta)k_{jk}\right\}. \tag{8}$$

So far we have given the diagonal elements of the relaxation matrix. The off-diagonal elements of the relaxation matrix, w_{jk}, are given by

$$w_{jk}=-\beta_\Pi\beta_\Delta k_{jk}\ \text{ for }\ (j-k)\ \text{ even},$$

and

$$w_{jk}=-(1-\beta_\Pi)(1-\beta_\Delta)k_{jk}\ \text{ for }\ (j-k)\ \text{ odd}. \tag{9}$$

Note that this form assumes that the percentage of ΔJ odd or even is independent of the rotational level.

A common approach, and one we use here, is to use measured broadening coefficients and Eq. (2) to fit for the a, b, and c parameters of the EPG model. Once these are fixed, the complete relaxation matrix may be determined (for given values of the β parameters) and either the entire spectrum can be calculated at all pressures, or one can directly calculate the weak mixing (low-pressure) parameters.

In the first round of fitting, we do not have the broadening coefficients. However, as is well known, these are largely band independent. Thus, we can use experimental values from another band and the expression in Eq. (8) to determine reasonable values for the a, b, and c parameters. We used broadening coefficients from the $20\,^00\leftarrow01\,^10$ band[7] (J even) and interpolated them to find values for odd J values. The weak line-mixing coefficients for our branch were calculated using a value of $\beta_\Pi=\beta_\Delta=0.5$. By fitting our low-density data using calculated weak line-mixing parameters, we can retrieve accurate values of the line strengths and approximate values of the broadening coefficients. With these new line strengths we refit the data to extract accurate broadening coefficients and approximate values of the weak mixing parameter. In a final step, we estimate the second-order mixing terms[34] using our broadening coefficients to determine new EPG parameters and refit again for the experimental widths and more accurate experimental values of the first-order mixing parameters. Here, β_Π and β_Δ are allowed to float. This entire procedure may be carried out using any model of the intrinsic line shape.

TABLE I. Frequencies in cm^{-1} and line strength in units of 10^{-24}/(molecule/cm^2) of CO_2 in the $12\,^20\leftarrow01\,^10$ Q branch at 296 K.

		Present experiment		HITRAN2000
J	Line position	$S_Q(J)$[a]	$S_Q(J)$[b]	$S_Q(J)$[c]
2	2093.346 577	1.26(6)	1.28(5)	1.25
3	2093.355 723	2.22(6)	2.24(5)	2.17
4	2093.350 674	2.92(6)	2.97(5)	2.96
5	2093.372 081	3.69(6)	3.72(5)	3.68
6	2093.357 109	4.38(6)	4.43(5)	4.34
7	2093.395 717	4.97(6)	4.99(5)	4.94
8	2093.365 874	5.36(6)	5.49(5)	5.48
9	2093.426 641	5.92(5)	5.93(4)	5.95
10	2093.376 963	6.32(6)	6.36(5)	6.35
11	2093.464 864	6.65(5)	6.70(4)	6.70
12	2093.390 364	6.82(6)	6.94(5)	6.97
13	2093.510 401	7.24(4)	7.30(3)	7.18
14	2093.406 065	7.18(5)	7.23(4)	7.32
15	2093.563 268	7.45(4)	7.55(3)	7.41
16	2093.424 049	7.33(5)	7.36(4)	7.42
17	2093.623 487	7.36(4)	7.37(3)	7.39
18	2093.444 299	7.42(5)	7.45(4)	7.29
19	2093.691 080	7.05(4)	7.12(3)	7.16
20	2093.466 793	6.88(6)	6.89(5)	6.98
21	2093.766 074	6.87(5)	6.92(4)	6.77
22	2093.491 505	6.48(6)	6.52(5)	6.51
23	2093.848 496	6.16(6)	6.20(5)	6.24
24	2093.518 407	5.82(6)	5.84(5)	5.93
25	2093.938 379	5.6(6)	5.63(5)	5.63
26	2093.547 466	5.33(5)	5.35(4)	5.29
28	2093.578 645	4.69(6)	4.70(5)	4.61
30	2093.611 903	3.98(6)	3.92(5)	3.95
32	2093.647 193	3.28(6)	3.29(5)	3.31
34	2093.684 462	2.68(6)	2.72(5)	2.73
36	2093.723 653	2.19(6)	2.17(5)	2.20
38	2093.764 700	1.77(6)	1.79(5)	1.75
40	2093.807 531	1.34(6)	1.35(5)	1.36
42	2093.852 068	1.03(6)	1.04(5)	1.04
44	2093.898 222	0.78(6)	0.79(5)	0.78
46	2093.945 898	0.58(6)	0.59(5)	0.58

[a]As determined by fits with the asymmetric Voigt profile.
[b]As determined by fits with the asymmetric speed-dependent Lorentz profile.
[c]As determined by fits with a Voigt profile and averaged over several bands.

Table I lists the line strengths (averaged over the low-pressure measurements) when we use either the Voigt or the speed-dependent Lorentz profile. There is a small dependence on the choice of spectral profile, but the results overlap within the quoted error bars. In the same table we have added the values given in HITRAN2000.[35] The data for HITRAN were determined from spectra fitted only with a Voigt profile. The two sets of data agree within 3% or better.

From the medium-pressure spectra (below 60 torr), we also retrieved the integrated band intensity. As in previous studies[6,7] we have fixed the relative line strengths to the val-

TABLE II. Broadening coefficients of pure CO_2 in cm^{-1}/atm.

J	Present experiment[a,b,c]			HITRAN2000[d]
2	0.1190(40)	0.1253(39)	0.1265(40)	0.1228
3	0.1154(35)	0.1220(34)	0.1223(36)	0.1204
4	0.1124(33)	0.1175(33)	0.1188(32)	0.1190
5	0.1100(25)	0.1138(24)	0.1158(23)	0.1154
6	0.1090(20)	0.1130(22)	0.1133(22)	0.1141
7	0.1080(18)	0.1105(19)	0.1112(20)	0.1128
8	0.1070(16)	0.1089(17)	0.1093(18)	0.1116
9	0.1055(10)	0.1070(9)	0.1077(10)	0.1103
10	0.1040(8)	0.1058(9)	0.1063(9)	0.1091
11	0.1030(7)	0.1045(7)	0.1052(7)	0.1079
12	0.1030(8)	0.1040(8)	0.1042(8)	0.1067
13	0.1012(7)	0.1030(7)	0.1031(7)	0.1055
14	0.1010(8)	0.1020(8)	0.1022(8)	0.1043
15	0.0988(7)	0.1010(6)	0.1013(6)	0.1032
16	0.0972(8)	0.1002(6)	0.1005(6)	0.1020
17	0.0965(7)	0.0996(5)	0.0997(5)	0.1009
18	0.0959(9)	0.0987(6)	0.0988(6)	0.0998
19	0.0953(7)	0.0980(6)	0.0981(6)	0.0987
20	0.0947(9)	0.0971(8)	0.0973(8)	0.0977
21	0.0940(8)	0.0962(5)	0.0964(5)	0.0966
22	0.0934(9)	0.0951(9)	0.0955(9)	0.0956
23	0.0928(8)	0.0944(8)	0.0947(8)	0.0946
24	0.0921(10)	0.0936(9)	0.0938(9)	0.0935
25	0.0915(8)	0.0926(8)	0.0929(8)	0.0926
26	0.0908(10)	0.0918(10)	0.0921(11)	0.0916
28	0.0887(12)	0.0900(11)	0.0903(12)	0.0897
30	0.0870(15)	0.0881(14)	0.0885(14)	0.0878
32	0.0853(20)	0.0862(20)	0.0866(20)	0.0860
34	0.0837(24)	0.0842(20)	0.0848(24)	0.0843
36	0.0822(24)	0.0828(24)	0.0831(26)	0.0826
38	0.0808(26)	0.0810(24)	0.0813(25)	0.0810
40	0.0795(26)	0.0795(26)	0.0797(24)	0.0795
42	0.0781(28)	0.0780(26)	0.0782(55)	0.0780
44	0.0762(32)	0.0763(28)	0.0766(28)	0.0765
46	0.0754(34)	0.0754(33)	0.0755(32)	0.0751

[a]First column, ad determined by fits with the asymmetric Voigt profile.
[b]Second column, as determined by fits with the asymmetric Lorentz profile.
[c]Third column, as determined by fits with the asymmetric speed-dependent Lorentz profile.
[d]HITRAN2000 uses a collection of results and assumes the widths to be band- and branch independent.

ues in Table I and floated the overall vibrational Q-branch intensity. Our vibrational band intensity 393.7(1) $\times 10^{-24}$ cm^{-1}/(molecule/cm^2) compares well with the 401 $\times 10^{-24}$ cm^{-1}/(molecule/cm^2) value obtained by Rinsland *et al.* from Fourier transform measurements.[36] (They were not able to retrieve intensities for the individual Q-branch transitions).

Table II lists the broadening coefficients extracted using a Voigt, Lorentz, and speed-dependent Lorentz model for the intrinsic spectral profile of an isolated line. When speed dependence of the broadening is included in the fitting profile, the term ''width'' loses precise meaning. The width reported here is the Boltzmann-averaged width and is generally designated as Γ_m in the literature.[37] The reported pressure broadening coefficients were determined from plots of the width versus pressure and are the slopes of lines that pass through zero. At pressures below 60 torr the asymmetric Voigt profile is very close to a pure Voigt profile, and these broadening coefficients may be compared with values obtained by Rinsland *et al.*[36] and those compiled in HITRAN2000.[35] The agreement is within 5%. However, as is evident from Fig. 3, the difference between our results and those given in HITRAN shows a systematic dependence on J and on the model used to fit the profiles. The systematic difference persists even when the Voigt profile is used for both sets of data. Clearly, the broadening coefficients are not totally band independent.

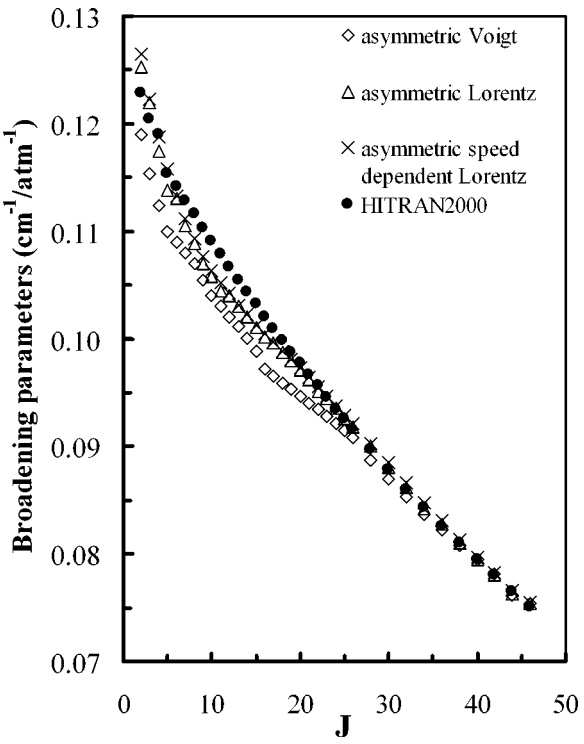

FIG. 3. Observed Q-branch broadening parameters as a function of J. The filled circles are the coefficients from HITRAN2000.

We now turn our attention to the weak mixing coefficients. They are given in Table III. They were retrieved from the spectral fits using the asymmetric speed-dependent Lorentz model. For each individual spectral line we have determined the mixing parameters, $y(J)$, by a linear regression of the fitted asymmetric component, $Y(J)$, versus pressure, forcing the fitted line to pass through the origin. The first column of results corresponds to experimental values obtained by neglecting the second-order mixing terms, G and H.[34] The second column presents values obtained by correcting the data using our estimated values of G and H (see Ref. 7). The second-order terms make a significant contribution to the mixing at our pressures. Note there is not the usual smooth evolution with J, being of one sign for low J and the opposite sign for high J. The irregular variation of the weak mixing coefficient with J [see Table III or Fig. 8(c) below] is real and arises because of the near overlap of lines belonging to different subbranches. This leads to large values ($\pm$) of the mixing coefficient only if collisions which couple the two subbranches (ΔJ odd) occur. As reported in studies of the pure CO_2 Q branches located at 2077 cm^{-1} (Ref. 6) and 2130 cm^{-1} (Ref. 7), we find that the sum rule, $\Sigma S_i Y_i = 0$, is violated. Again, we attribute this to the neglect of interbranch mixing in our fitting routines.

As outlined above, extracting the line strengths, broad-

TABLE III. Weak line-mixing coefficients in units atm^{-1}, for transitions of the Q branch of pure CO_2 in the $12\,^20 \leftarrow 01\,^10$ Q branch at 296 K.

	Expt.		Calcd.
J	a	b	c
2	8.021(20)	8.284(19)	8.231
3	5.871(18)	5.998(18)	5.685
4	4.411(15)	4.334(16)	4.199
5	−0.668(14)	−0.541(14)	−0.527
6	−1.929(14)	−1.726(14)	−1.609
7	−1.544(11)	−1.559(12)	−1.472
8	1.380(14)	1.494(14)	1.416
9	−2.218(12)	−2.333(12)	−2.188
10	−0.187(12)	−0.213(12)	−0.201
11	0.708(10)	0.851(10)	0.786
12	0.902(12)	0.979(12)	0.911
13	−0.385(10)	−0.387(10)	−0.367
14	−0.016(12)	−0.035(12)	−0.041
15	−0.445(10)	−0.481(10)	−0.454
16	1.255(12)	1.354(12)	1.254
17	−0.408(11)	−0.449(11)	−0.424
18	0.012(12)	0.010(12)	−0.001
19	−0.367(11)	−0.410(11)	−0.388
20	−1.323(12)	−1.495(12)	−1.407
21	−0.445(11)	−0.498(11)	−0.473
22	0.021(12)	0.019(12)	0.007
23	−0.173(11)	−0.190(11)	−0.181
24	−0.286(12)	−0.342(12)	−0.331
25	−0.171(12)	−0.190(12)	−0.182
26	0.031(12)	0.033(12)	0.020
28	−0.148(13)	−0.173(13)	−0.173
30	0.053(13)	0.060(12)	0.046
32	−0.101(14)	−0.119(14)	−0.122
34	0.113(14)	0.140(14)	0.123
36	−0.081(15)	−0.095(14)	−0.099
38	0.656(16)	0.739(16)	0.694
40	−0.072(18)	−0.082(17)	−0.086
42	−0.291(21)	−0.344(19)	−0.337
44	−0.067(22)	−0.078(21)	−0.081
46	−0.150(23)	−0.182(22)	−0.182

[a]Experimental results obtained ignoring the second-order line-mixing terms.
[b]Experimental results obtained including the second-order line-mixing terms.
[c]Coefficients calculated from present broadening coefficients assuming that the relative amounts of even–even and even–odd couplings are independent of J.

ening, and weak mixing coefficients from the data uses an EPG model to correct for higher order terms in the mixing, the coefficients for the EPG law being determined from the measured broadening curves. When we use the broadening coefficients retrieved using the asymmetric Lorentz model to determine the EPG coefficients, we find, $\beta_\Pi = 0.46$, $\beta_\Delta = 0.675$, $a = 0.0391$, $b = 0.214$, $c = 1.404$.

Here, we can use the fitted EPG coefficients, or the corresponding coefficients for the ECS model described below, to understand the anatomy of line mixing and thus to understand at least qualitatively the overall collapse of the band with pressure. [See Fig. 1(b)]. As indicated in the Introduction, given a relaxation matrix, it is possible to decompose the band into a sum of spectral components, each expressed as the sum of a symmetric and an asymmetric Lorentzian component [see Eq. (3)]. The results are shown in Figs. 4(a)–4(d), where we have labeled the spectral components according to their low-pressure identity assuming continuity of the curves.

Figure 4(a) shows the computed intensity of the spectral components as a function of pressure. The most striking feature of this figure is the fact that the intensity of all spectral components except one, here Q(8), falls to zero at high pressure. This dominant component assumes all of the Q-branch intensity. The computed curves for the frequencies, widths, and asymmetries [Figs. 4(b), 4(c), and 4(d)] all show this component as a darkened curve. In Figs. 4(a), 4(c), and 4(d), we have actually plotted S_k/P, Γ_k/P, and Y_k/P, respectively. Thus, we expect the curves to approach constant line strengths, broadening, and mixing coefficients, respectively, as the pressure is lowered towards zero. However, it is the behavior at high pressures that is of interest.

Figure 4(d) shows that the asymmetry of the Q(8) spectral component vanishes at high pressure. Thus, from Figs. 4(a), 4(b), and 4(d), we expect the band to become a single Lorentzian with a width given by the width of the Q(8) component of Fig. 4(c). We have fitted the collapsing $12\,^20 \leftarrow 01\,^10$ Q branch with an asymmetric Lorentzian model and find the quality of the fit to be excellent [see Fig. 5(a)].

The question is ''How do the fitted parameters compare with the computed parameters for Q(8)?'' A visual examination of the peak position in Fig. 1(b) shows it to be comparable to computed shift in the Q(8) component shown in Fig. 4(b). Thus, it is line mixing and not a shift in the vibrational frequency, that dominates the displacement of the strongly mixed Q branch. As shown in Figs. 5(b) and 5(c), the agreement between the calculated and fitted values does not extend to the width and asymmetry. Figure 4(a) suggests the values should converge rapidly above 2 atm. However, the widths appear to diverge with the measured profile having a width less than the computed Q(8) width, above about 6 atm. The computed asymmetry is larger than the fitted asymmetry, although there appears to be slow convergence of the two values as the pressure is increased. While part of the numerical disagreement of the two asymmetries can be ascribed to the neglect of interbranch mixing, it is unlikely that this also causes the 10% disagreement in the widths. While such accuracy may be adequate for atmospheric modeling, the EPG model suffers from the drawback that the data for each band must be available in order to determine the model parameters. In other words, the EPG law applies band by band rather than globally for all bands of a given molecule. The ECS model overcomes this limitation.

III. PART II: ECS ANALYSIS OF THE $20\,^00 \leftarrow 01\,^10$, $11\,^10 \leftarrow 00\,^00$, AND $12\,^20 \leftarrow 01\,^10$ Q BRANCHES

Part I completes our experimental study of three Q branches in the infrared spectrum of pure CO_2, all at room temperature. In Ref. 6 the band at 2077 cm^{-1} was a $\Pi \leftarrow \Sigma$ transition. In Ref. 7 the band at 2130 cm^{-1} was a $\Sigma \leftarrow \Pi$ transition. In the present paper, the band is located at 2093 cm^{-1} and is a $\Delta \leftarrow \Pi$ transition. In the last case both the upper and lower states have nonzero vibrational angular momentum. In all three studies we used some form of an EPG law either in the extraction of the width and the weak mixing coefficient from the data or in modeling the band for strong

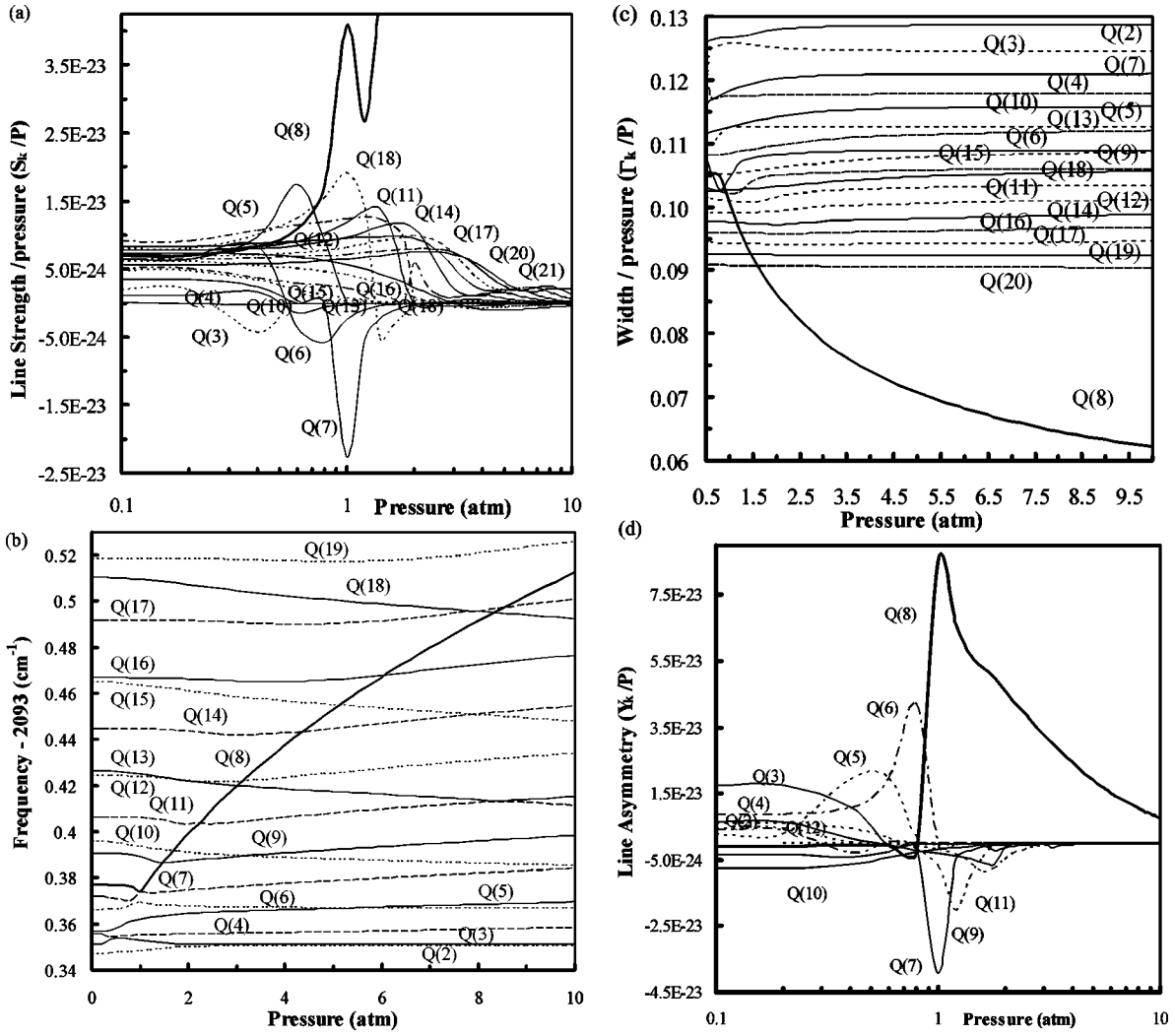

FIG. 4. As calculated from inversion of the relaxation matrix, the pressure dependence of (a) strength of the components; (b) frequency of the components; (c) width of the components, divided by pressure; (d) asymmetry of the components, divided by pressure.

mixing. We did this band by band and "played" with the problem of deciding whether or not to include ΔJ odd or even (rotational) parity changing collisions. In this section we examine the suitability of the ECS model for describing all bands with one set of fitted parameters. The ECS model addresses the question of (rotational) parity changes directly. In the Introduction we outlined a general formalism for determining band shapes which has, as an important ingredient, the relaxation matrix *w*. All that remains is to describe how the ECS relaxation matrix is constructed.

Recall that since collisional transfer rates between levels in different vibrational states are extremely small, only the *w* elements connecting rotational transitions within a given band are accounted for. Furthermore, since the off-diagonal imaginary elements are expected to be very small and in the absence of any model for their construction, only the real part of *w* is constructed. Within the approximations detailed in Ref. 4, the ECS expression of the *w* element connecting two lines ($j_f' \leftarrow j_i'$ and $j_f \leftarrow j_i$) of the $\nu_{1f}\nu_{2f}^{l_f}\nu_{3f} \leftarrow \nu_{1i}\nu_{2i}^{l_i}\nu_{3i}$ vibrational band is given by

$$\langle\langle j_i' l_i j_f' l_f | w(T) | j_i l_i j_f l_f \rangle\rangle = (2j_i'+1)\sqrt{(2j_f+1)(2j_f'+1)}(-1)^{l_i+l_f} \times \sum_{L\,\mathrm{even}\neq 0} \begin{pmatrix} j_i & L & j_i' \\ l_i & 0 & -l_i \end{pmatrix} \begin{pmatrix} j_f & L & j_f' \\ -l_f & 0 & l_f \end{pmatrix} \begin{Bmatrix} j_i & j_f & 1 \\ j_f' & j_i & L \end{Bmatrix} \times (2L+1)) \frac{\Omega(j_i,T)}{\Omega(L,T)} Q(L,T), \quad (10)$$

where $(\cdots)$ and $\{\cdots\}$ are 3J and 6J coefficients.[38] Note that Eq. (10) is used for "downward" transitions ($j_i' < j_i$) only, the upward ones being obtained from detailed balance, i.e.,

$$\langle\langle j_i l_i j_f l_f | w(T) | j_i' l_i j_f' l_f \rangle\rangle = \frac{\rho_{j_i}(T)}{\rho_{j_i'}(T)} \langle\langle j_i' l_i j_f' l_f | w(T) | j_i l_i j_f l_f \rangle\rangle. \quad (11)$$

In Eq. (10), an adiabaticity factor is defined by[39]

$$\Omega(j,T) = \left\{ 1 + \frac{1}{24}\left[\frac{\omega_{j,j-2} d_c}{\overline{\nu}(T)} \right]^2 \right\}^{-2}, \quad (12)$$

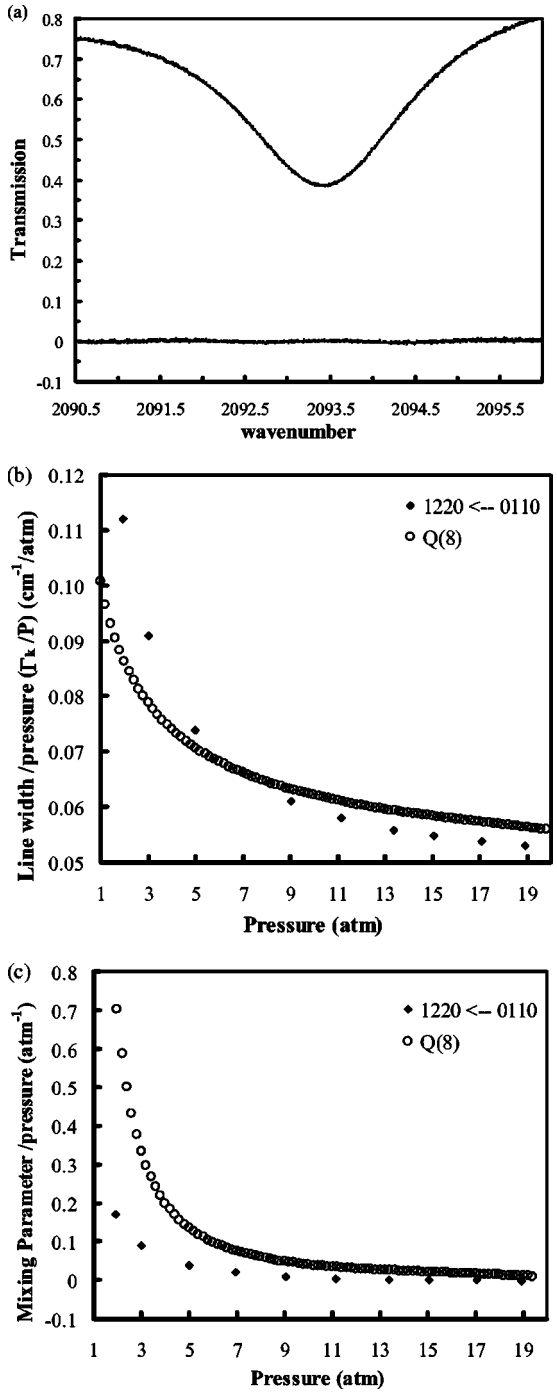

FIG. 5. (a) Q branch spectrum recorded at 19 atm and fit residual using the asymmetric Lorentzian profile and a comparison of (b), the fitted width divided by pressure with corresponding value for the Q(8) component and (c) the fitted asymmetry divided by pressure with the corresponding value for Q(8).

where $\omega_{j,j-2}$, $\overline{\nu}$, d_c are the frequency spacing between level j and $j-2$, the mean relative velocity in CO_2-CO_2 collisions, and the scaling length. As widely done before, the basic rates are expressed through an exponential power law[40]

$$Q(j,T)=A(T)[L(L+1)]^{-\lambda(T)}\exp\left[-\beta(T)\frac{hcE_j}{k_BT}\right], \tag{13}$$

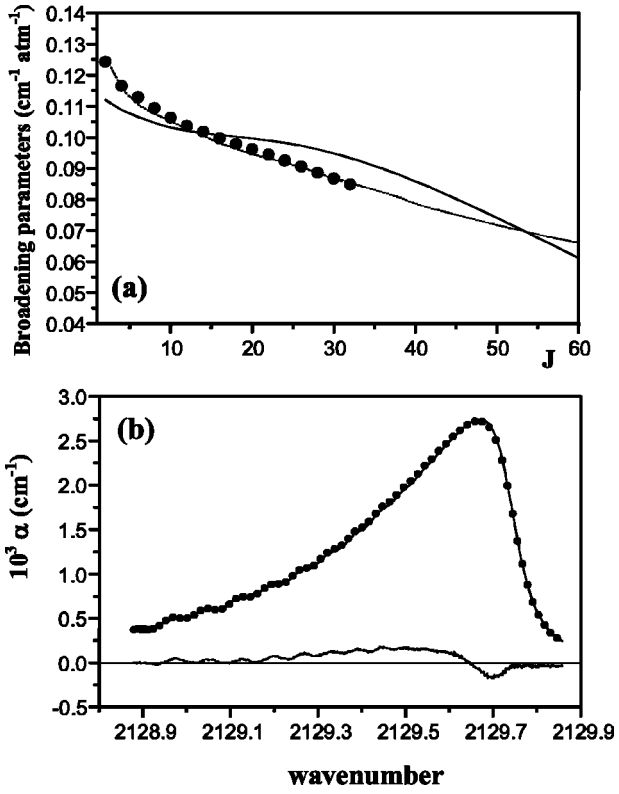

FIG. 6. Comparisons between ECS-EP predictions (continuous line) and measured values (black dots). (a) Low-pressure self broadening coefficients of Q lines [the reference values, from HITRAN (Ref. 35) have been validated in Ref. 6]. (b) Absorption in the $20^00\leftarrow01^10$ Q branch for 400 torr (the lower curve gives the measured–calculated deviations multiplied by 5).

where E_j is the rotational energy of level j. The quantities d_c, A, λ, and β are the only parameters of the ECS-EP model. Their knowledge enables the construction of w for any band. The data required for the computation of a band profile are, for each line k, the line identification (rotational and vibrational quantum numbers), position σ_k, dipole transition moment d_k, energy of the lower level E_k, and the ECS law parameters. The first (spectroscopic) quantities have been taken from the 2000 edition of the HITRAN database.[35] Here, the collisional parameters d_c, A, λ, and β have been determined from a fit of line-broadening data using Eq. (2), but, as was done in Ref. 41, this fit was carried out "keeping an eye" on the 2130 cm^{-1} ($20^00\leftarrow01^10$) Q-branch profile at 400 torr in order to obtain parameters that lead to simultaneous satisfactory agreement with measurements for both the broadening and the Q branch shape [Figs. 6(a) and 6(b)]. The ECS parameters are temperature dependent. Here, we use only room temperature results as these are the only ones that are available. We find the room temperature parameters to be $A=0.018\ cm^{-1}/atm$, $\lambda=0.74$, $\beta=0.06$, and $d_c=6.0$ Å. How well these parameters reproduce the input broadening coefficients and absorption spectrum is illustrated in Figs. 6(a) and 6(b). As for CO_2-N_2,[41] excellent agreement with the measured absorption spectrum is obtained while the quality of predicted half-widths is better than 10% (the intensity weighted rms is 6%).

To illustrate the universality of the ECS model, Fig. 7 shows a comparison of computed and measured absorption

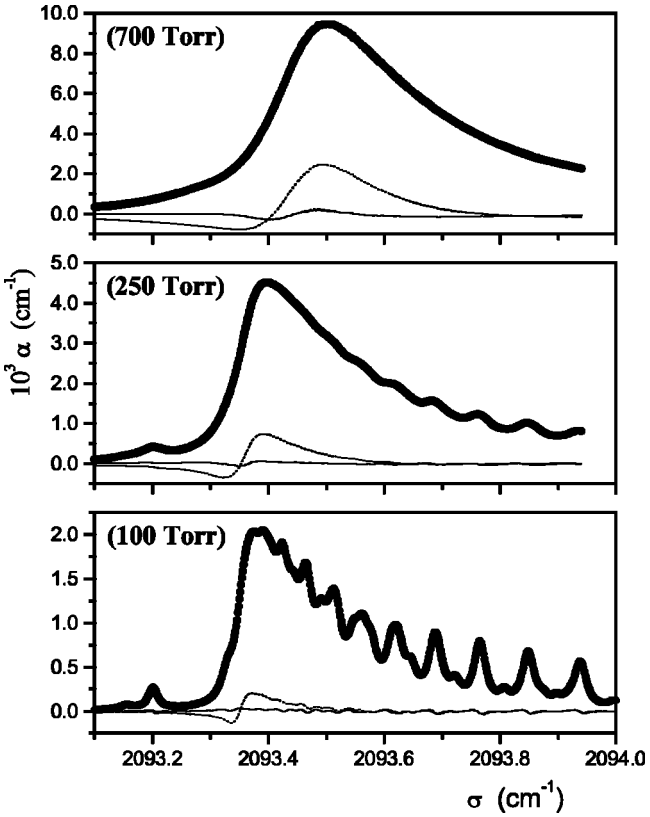

FIG. 7. Absorption in the $12\,^20\leftarrow01\,^10$ Q branch for various pressures. In each panel there are measured (difference frequency) values, whereas ——— and --- are measured–calculated deviations obtained with the ECS-EP model, respectively, accounting for and neglecting line mixing.

spectra of the present band at 2093 cm^{-1}, for several pressures. Included in the figure is a plot of the residuals, i.e., the difference between the calculated and observed spectra. Similar results were found for the 2077 cm^{-1} Q branch as well as for the 2130 cm^{-1} Q branch at pressures other than 400 torr.

It is remarkable that a single set of ECS parameters is able to reproduce the band shapes of all three bands. Note that this is quite a success since the absorption is very well

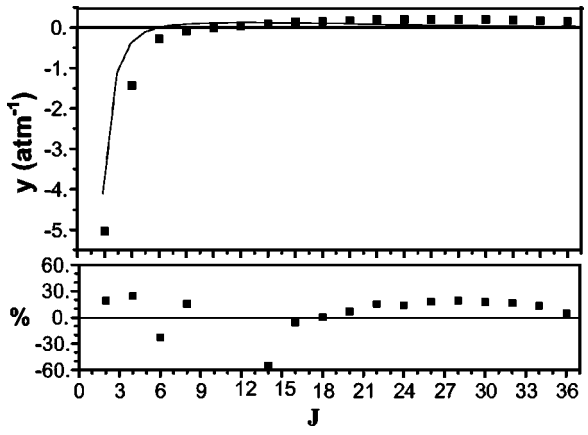

FIG. 8. (a) Line-mixing coefficients in the $20\,^00\leftarrow01\,^10$ Q branch. ■ are values derived from measured spectra (Ref. 7), whereas ——— have been calculated with the ECS-EP model. Measured–calculated relative deviations are given in the lower part.

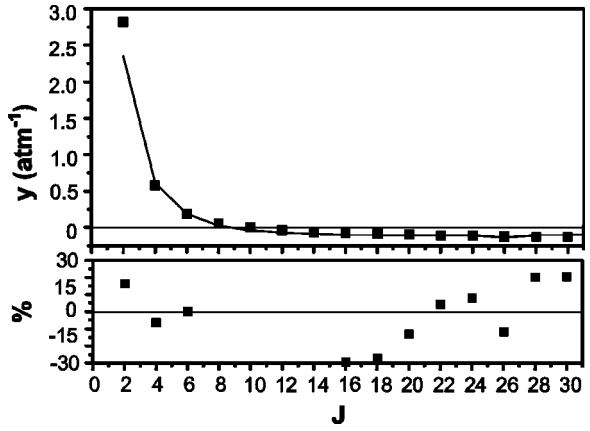

FIG. 9. As in Fig. 8, but for the $11\,^10\leftarrow00\,^00$ Q lines. The measured values are from Ref. 6.

predicted, although the three transitions under study have different symmetries ($\Sigma\leftarrow\Pi$, $\Pi\leftarrow\Sigma$, and $\Delta\leftarrow\Pi$) and spectral structures. In particular, as noted above, the 2093 cm^{-1}, $\Delta\leftarrow\Pi$ band includes lines of even and odd J values. This confirms the ability of the ECS approach to account for the effects of the vibrational angular momenta.[33,42]

Another interesting test of the model can be made by comparing the first-order line-mixing coefficients Y_k retrieved from measured spectra with those from the ECS-EP relaxation matrix and Eq. (5). Such comparisons for the Q lines of the three Q branches under study are plotted in Figs. 8 to 10. They confirm the quality of the model. In particular, the values for odd and even J values are correctly predicted as are the oscillations due to coincidences between positions of odd and even Q(J) lines in Fig. 10. The values in Figs. 8 and 9 enable a further test of the model. Indeed, according to Eq. (10) the off-diagonal elements of W coupling Q lines should be the same in the $11\,^10\leftarrow00\,^00$ [$\Pi\leftarrow\Sigma,\ell_I=0,\ell_f=1$] and $20\,^00\leftarrow01\,^10$ [$\Sigma\leftarrow\Pi,\ell_1=1,\ell_f=0$] bands. Since the positions of the Q lines of moderate J values can be well approximated by $\sigma_{Q(J)}=\sigma_{vib}+J(J+1)\Delta B_{vib}$, where σ_{vib} is the vibrational frequency and ΔB_{vib} the difference of the rotational constants in the upper and lower states, one can

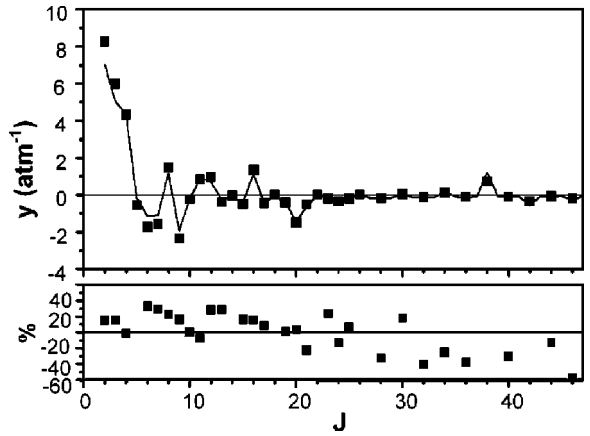

FIG. 10. As in Fig. 8, but for the $12\,^20\leftarrow01\,^10$ Q lines. The measured values are from Ref. 7.

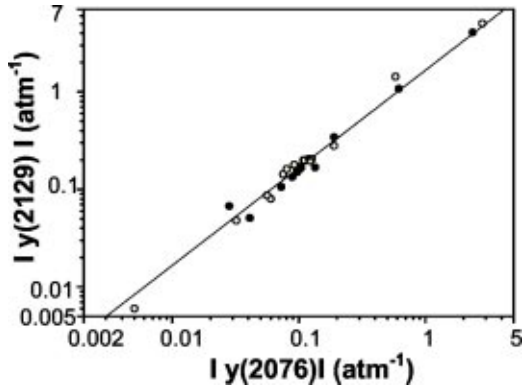

FIG. 11. Absolute values of the line-mixing coefficients of Q lines in the $20\,^0 0 \leftarrow 01\,^1 0$ band versus those in the $11\,^1 0 \leftarrow 00\,^0 0$ band. The closed and open circles are calculated and measured values, respectively. The straight line corresponds to the law in Eq. (14).

easily show from Eq. (5) that the line coupling coefficients, y, in the two bands should satisfy

$$y_J(2130) = \frac{\Delta B_{2077}}{\Delta B_{2130}} y_J(2077) = -1.66 y_J(2077). \qquad (14)$$

Figure 11 confirms that the W elements connecting Q lines are the same for $\Pi \leftarrow \Sigma$ and $\Sigma \leftarrow \Pi$ bands.

IV. CONCLUSIONS

In summary we have studied the behavior of the 2093 cm^{-1} Q branch of CO_2 over a wide range of pressures, all at room temperature. The low-pressure spectra, recorded with a difference frequency system, were analyzed using a variety of line shape models that included weak line mixing. This yielded the line and branch strengths, as well as the broadening and weak mixing coefficients. An EPG law was used to understand the nature of the collapse of the band recorded with an FTIR spectrometer at high pressures. In the last part of the paper we have demonstrated that a single ECS model of the relaxation matrix provides a unified description not only of the mixing and band collapse of the present band but also of the Q branches at 2077 cm^{-1} and 2130 cm^{-1} reported in earlier publications.

ACKNOWLEDGMENTS

A.P.-C. acknowledges support from the University of Lethbridge Start-up Research Grant and from the University of Toronto. A.V. was supported by funding from the Natural Sciences and Engineering Research Council of Canada, COMDEV, Bomem Inc., Atmospheric Environment Service, University of Toronto Research Fund and the Canadian Space Agency. Our gratitude also goes to Richard Berman for numerous fruitful discussions in the early stages of this project.

[1] A. Lévy, N. Lacome, and C. Chackerian Jr., *Spectroscopy of the Earth Atmosphere and Interstellar Medium*, 261 (Academic, New York, 1992).
[2] C. P. Rinsland and L. L. Strow, Appl. Opt. **28**, 457 (1989).
[3] L. L. Strow, D. C. Tobin, and S. E. Hannon, J. Quant. Spectrosc. Radiat. Transf. **52**, 281 (1994).
[4] R. Rodrigues, K. W. Jucks, N. Lacome *et al.*, J. Quant. Spectrosc. Radiat. Transf. **61**, 153 (1999).
[5] K. W. Jucks, R. Rodrigues, R. Le Doucen, C. Claveaux, and J. M. Hartmann, J. Quant. Spectrosc. Radiat. Transf. **63**, 31 (1999).
[6] R. Berman, P. Duggan, P. M. Sinclair, A. D. May, and J. R. Drummond, J. Mol. Spectrosc. **182**, 350 (1997).
[7] A. Predoi-Cross, C. Luo, R. Berman, J. R. Drummond, and A. D. May, J. Chem. Phys. **112**, 8367 (2000).
[8] R. L. Armstrong, Appl. Opt. **21**, 2141 (1982).
[9] L. L. Strow and B. M. Gentry, J. Chem. Phys. **84**, 1149 (1986).
[10] T. Huet, N. Lacome, and A. Levy, J. Mol. Spectrosc. **138**, 141 (1989).
[11] L. Bonamy, J. Bonamy, S. Temkin, D. Robert, and J. M. Hartmann, J. Chem. Phys. **98**, 3747 (1993).
[12] M. Margottin-Maclou, F. Rachet, C. Boulet, A. Henry, and A. Valentin, J. Mol. Spectrosc. **172**, 1 (1995).
[13] J. M. Hartmann, C. Boulet, M. Margottin-Maclou, F. Rachet, B. Khalil, F. Thibault, and J. Boissoles, J. Quant. Spectrosc. Radiat. Transf. **54**, 705 (1995).
[14] N. N. Filippov and M. V. Tonkov, J. Quant. Spectrosc. Radiat. Transf. **50**, 111 (1993).
[15] B. Gentry and L. L. Strow, J. Chem. Phys. **86**, 5722 (1987).
[16] L. Bonamy and F. Emond, Phys. Rev. A **51**, 1235 (1995).
[17] S. Green, J. Chem. Phys. **90**, 3603 (1989).
[18] J.-P. Bouanich, R. Rodrigues, and C. Boulet, J. Quant. Spectrosc. Radiat. Transf. **54**, 683 (1995).
[19] J. P. Bouanich, J. M. Hartmann, Gh. Blanquet, J. Walrand, D. Bermejo, and J. L. Domenech, J. Chem. Phys. **109**, 6684 (1998).
[20] G. Blanquet, J. Walrand, and J.-P. Bouanich, J. Mol. Spectrosc. **210**, 1 (2001).
[21] S. Hadded, F. Thibault, P. M. Flaud, H. Aroui, and J. M. Hartmann, J. Chem. Phys. **116**, 7544 (2002).
[22] J. M. Hartmann and C. Boulet, J. Chem. Phys. **94**, 6406 (1991).
[23] B. Lance and D. Robert, J. Chem. Phys. **109**, 8283 (1998).
[24] S. Pine and T. Gabard, J. Quant. Spectrosc. Radiat. Transf. **66**, 69 (2000).
[25] A. Ben-Reuven, Phys. Rev. **145**, 7 (1966).
[26] J. M. Hartmann, R. Rodrigues, Nguyen-Van-Thanh, C. Brodbeck, C. Boulet, R. Le Doucen, N. Lacome, and L. Bonamy, J. Chem. Phys. **110**, 7733 (1999).
[27] A. D. May, Phys. Rev. **59**, 3495 (1999).
[28] R. G. Gordon and R. P. McGinnis, J. Chem. Phys. **49**, 2455 (1968).
[29] P. W. Rosenkranz, IEEE Trans. Antennas Propag. **AP-23**, 498 (1975).
[30] P. Duggan, P. M. Sinclair, M. P. LeFlohic, J. W. Forsman, R. Berman, A. D. May, and J. R. Drummond, Phys. Rev. A **48**, 2077 (1993).
[31] G. Herzberg, *Infrared and Raman Spectra of Polyatomic Molecules* (Van Nostrand, New York, 1945).
[32] P. Bernath, *Spectra of Atoms and Molecules* (Oxford University Press, New York, 1995).
[33] R. Rodrigues, Gh. Blanquet, J. Walrand, B. Khalil, R. Le Doucen, F. Thibault, and J. M. Hartmann, J. Mol. Spectrosc. **186**, 256 (1997).
[34] E. W. Smith, J. Chem. Phys. **74**, 6658 (1981).
[35] L. S. Rothman, A. Barbe, and D. C. Benner, J. Quant. Spectrosc. Radiat. Transf. **82**, 5 (2003).
[36] C. P. Rinsland, D. C. Benner, and V. Malathy Devi, Appl. Opt. **25**, 1204 (1986).
[37] R. Berman, P. M. Sinclair, A. D. May, and J. R. Drummond, J. Mol. Spectrosc. **198**, 278 (1999).
[38] A. R. Edmonds, *Angular Momentum in Quantum Mechanics* (Princeton University Press, Princeton, NJ, 1974).
[39] A. E. DePristo, S. T. Augustin, R. Ramaswamy, and H. Rabitz, J. Chem. Phys. **71**, 850 (1979).
[40] G. Millot, J. Chem. Phys. **93**, 8001 (1990).
[41] R. Rodrigues, B. Khalil, R. Le Doucen, L. Bonamy, and J. M. Hartmann, J. Chem. Phys. **107**, 4118 (1997).
[42] J. P. Bouanich, R. Rodrigues, J. M. Hartmann, J. L. Domenech, and D. Bermejo, J. Mol. Spectrosc. **186**, 269 (1997).